

Noise Tolerant Quantum Algorithm for Ground State Energy Estimation

Erenay Karacan,^{1,*} Yanbin Chen,^{2,†} and Christian B. Mendl^{2,3,‡}

¹*Technical University of Munich, CIT, Department of Electrical Engineering and Information Technology, Arcisstraße 21 80333 Munich, Germany*

²*Technical University of Munich, CIT, Department of Computer Science, Boltzmannstraße 3, 85748 Garching, Germany*

³*Technical University of Munich, Institute for Advanced Study, Lichtenbergstraße 2a, 85748 Garching, Germany*

(Dated: May 20, 2024)

One of the most promising applications of quantum computers is to simulate physical systems, leveraging their inherent quantum behavior to achieve an advantage over classical computation. In this work, we present a noise-tolerant Hamiltonian simulation algorithm for ground-state energy estimation. Our method surmounts stochastic sampling limitations to estimate expectation values. It is based on an adaptive sequence of fuzzy bisection searches to estimate the ground state energy digit by digit, with a trade-off between increasing the simulation time and decreasing the absolute error rate. It builds upon the Quantum Eigenvalue Transformation of Unitary Matrices (QETU) algorithm, and it delivers good approximations in simulations with local, two-qubit gate depolarizing probability up to 10^{-3} , specifically for Hamiltonians that anti-commute with a Pauli string. To demonstrate the key results in this work, we ran simulations with different system Hamiltonians, system sizes, and time evolution encoding methods on classical computers using `Qiskit`. We compare the performance with other existing methods and show that we can consistently achieve two to three orders of magnitude improvement in the absolute error rate.

I. INTRODUCTION

Computing the ground state and its associated energy of a quantum Hamiltonian is a fundamental task in quantum science, with broad applications in condensed matter physics and chemistry. This task counts towards the natural application domain of (future) quantum computers. Although some of the proposed algorithms deliver promising results [1–9], they all inevitably face one major challenge in the current era of Noisy Intermediate-Scale Quantum (NISQ) devices: low tolerance of noisy hardware. Recently, a “fuzzy” bisection algorithm has been proposed for this purpose [2], combining interval search with eigenvalue filtering as enabled by the quantum signal processing framework [10]. Simultaneously, Ref. [2] substitutes the Hamiltonian block-encoding by the unitary time evolution operator, which is likely more straightforward to realize (via Trotterization) than the conventional block-encoding, particularly in the early fault-tolerant regime. While Ref. [2] achieves near-optimal theoretical complexity, a general difficulty is the increasing polynomial degree (and corresponding circuit depth) when approximating a sharp (step-like) transition to locate the eigenvalue. In this work, we alleviate these difficulties by retaining a fixed polynomial degree at the cost of larger evolution times. Specifically, we propose and study an *adaptive* fuzzy bisection search, which can iteratively determine the sought eigenvalue digit-by-digit. In the simulations, we employed different methods of simulating the time evolution of the quantum system and also ran the algorithms under different noise levels.

In our results we demonstrate that this approach can get to any arbitrary target precision if we assume early-fault tolerant hardware and can still achieve meaningful results when simulated with two-qubit gate depolarizing probability of up to 10^{-3} .

The main aim of our work is to extract the eigenvalue information from an end state prepared through Hamiltonian simulation, whose state fidelity to the ground state of the system Hamiltonian is sufficiently large $\langle \psi_{End} | \psi_0 \rangle \approx 1$. Previous works and our simulations demonstrate that this is achievable by using the “Quantum Eigenvalue Transformation of Unitary Matrices (QETU)” algorithm [2], proposed by Dong et al. if we repeat the QETU circuit layer three to five times for some of the most commonly used system Hamiltonians, such as the Ising and Heisenberg models. Implementation of the QETU circuit is visualized in Fig. 1.

To read out the eigenvalue corresponding to the prepared end state $\langle \psi_{End} | H | \psi_{End} \rangle$, different methods have been proposed such as the direct expectation value measurement [2], Quantum Complex Exponential Least Squares Algorithm (QCELS) [1] and using the so-called “fuzzy bisection search”, conducted through applying one additional QETU circuit layer after ground state preparation [2]. We simulate these approaches with different noise levels, in order to benchmark the performance of our proposed algorithm.

II. BACKGROUND

A. Fundamentals of QETU

As given in Theorem 1 of [2], QETU circuit with symmetric phases $\vec{\phi} \in \mathbb{R}^{\eta+1}$ optimized for a target polynomial $F(a)$, applied to a given input state $|\psi\rangle$ delivers the

* erenay.karacan@tum.de

† yanbin.chen@tum.de

‡ christian.mendl@tum.de

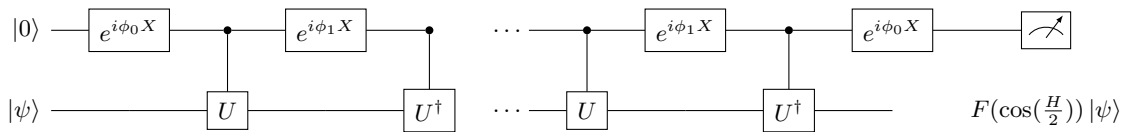


FIG. 1. Quantum Eigenvalue Transformation of Unitary Matrices (QETU) Circuit in compact notation where U is the multi-qubit gate applying the time evolution operator $U = e^{-iH}$, acting on all the system qubits and the X-Rotation gates are applied to the ancilla qubit. Symmetric phases $(\phi_0, \phi_1, \dots, \phi_1, \phi_0) \in \mathbb{R}^{\eta+1}$ are optimized for a given target polynomial $F(a)$.

following probability amplitude of measuring $|0\rangle$ at the ancilla qubit:

$$\begin{aligned} & (\langle 0| \otimes \langle \psi|) \mathcal{U}_{\text{QETU}} (|0\rangle \otimes |\psi\rangle) \\ &= \langle \psi| F(\cos(H/2)) |\psi\rangle = \sum_j |c_j|^2 F(\cos(\lambda_j/2)), \end{aligned} \quad (1)$$

where $\{\lambda_j, \psi_j\}_j$ is the spectrum of the Hamiltonian and $c_j = \langle \psi | \psi_j \rangle$ is the overlap of the initial state with the eigenstate $|\psi_j\rangle$. Here, $F(a)$ has to be real, have parity $\eta \bmod 2$, have the degree $\leq \eta$ and $|F(a)| \leq 1, \forall a \in [-1, 1]$.

As direct consequence of (1), applying QETU to an almost perfectly prepared ground state $|\tilde{\psi}\rangle$ delivers the success probability (measuring $|0\rangle$ at the ancilla qubit) of:

$$\left| (\langle 0| \otimes \langle \tilde{\psi}|) \mathcal{U}_{\text{QETU}} (|0\rangle \otimes |\tilde{\psi}\rangle) \right|^2 \approx |F(\cos(\lambda_0/2))|^2. \quad (2)$$

B. Fuzzy Bisection Search

We can use the QETU circuit to conduct a search to approximate the ground state energy, as Dong et al. proposed [2]. At each step of this "fuzzy bisection search", we apply one QETU layer with phases optimized for an even step polynomial $F(a)$ with cut-off value μ chosen depending on the current search step to determine whether the ground state energy, transformed into the cosine-space: $a_0 := \cos(\frac{\lambda_0}{2})$ is located in the upper or the lower half of the current search interval, hence cutting the search interval by approximately half after each successful search stage. What makes this search "fuzzy" and also the reason why the interval is not cut down exactly by half after each search stage, is because we take the non-ideal step behaviour of the approximated polynomial into account and update the new interval lower/upper bound to be $(\mu \mp \epsilon)$, where the tolerance parameter ϵ is chosen depending on the degree of the polynomial.

Measuring $|0\rangle$ with a high probability at the ancilla qubit, tells us that the a_0 is located in the upper half of the search interval, as it follows from (2) for a good approximate of the ground state $|\tilde{\psi}\rangle \approx |\psi_0\rangle$.

Main challenge of this approach is to increase the polynomial degree after each search stage to get a sharper step that can get more and more precise. This increases the complexity of optimizing the QSP phases exponentially

and empirically shown to be not achievable for polynomial degrees above 34 in our results.

An example fuzzy bisection search is visualized in Fig. 2.

III. ADAPTIVE FUZZY BISECTION SEARCH

The novel approach we propose in this project builds upon the idea of using the QETU circuit in a fuzzy bisection search, to better estimate the ground state energy from the almost perfectly prepared ground state, by breaking the approximation error lower bound caused by the stochastic limitation in the noiseless case and by increasing the tolerance of depolarizing noise.

Extracting the eigenvalue information from the prepared ground state through this "Adaptive Fuzzy Bisection" search is based on a set of fuzzy bisection search stages where each search stage corresponds to a target digit d on a chosen basis b . To achieve this, each search stage is conducted with a linear transformation of the system Hamiltonian:

$$\tilde{H} := c_1 H + c_2 I. \quad (3)$$

where the (c_1, c_2) pair is dependent on the outcome of the previous search as:

$$c_1 = \frac{\pi}{b^d} \quad c_2 = -c_1 \lambda_{LB}^d \quad (4)$$

where d is the target digit ($d \leq 0$ after floating point) and λ_{LB}^d is a lower bound estimate for the ground state energy, that can be systematically defined dependent on the search result λ_{d+1}^* of the previous stage ($d+1$):

$$\lambda_{LB}^d := \lambda_{d+1}^* - b^d. \quad (5)$$

This choice of c_1, c_2 implies the following relation between the transformed $a := \cos(\frac{\lambda}{2})$ space and λ space:

$$a := \cos(\frac{\pi}{2}(\lambda - \lambda_{LB}^d)b^{-d}) \quad (6)$$

The level of precision of λ_{LB}^d depends on the current search stage d , hence the subtraction $(\lambda - \lambda_{LB}^d)$ "gets rid" of the already correctly identified digits. Multiplication by b^{-d} magnifies or "zooms into" the target digit.

Before moving further, we define the result of subtraction and magnification as a helper variable:

$$x_d(\lambda) := (\lambda - \lambda_{LB}^d)b^{-d}. \quad (7)$$

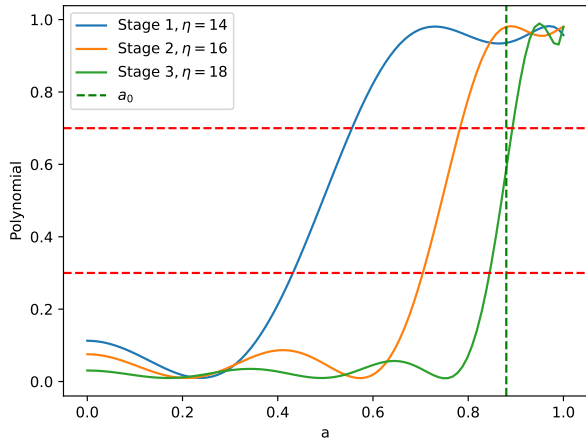


FIG. 2. An example fuzzy bisection search (with increasing polynomial degrees η), that lasted three stages. Search is terminated once the probability of measuring $|0\rangle$ at the ancilla qubit is above (or below) a certain threshold, indicating we reached the maximum achievable precision with the given (maximal) polynomial degree. In the example search, the threshold probabilities are set to 0.7 and 0.3 (indicated by the red lines).

Theorem. Assuming each Adaptive Fuzzy Bisection Search stage with search base $b \in \mathbb{R}$ can yield an estimation result $x_d^* := (\lambda_d^* - \lambda_{LB}^d)b^{-d}$ satisfying $|x_d^* - x_d(\lambda_0)| < b^{-1}$, $\forall d \in \mathbb{Z}$, each search stage requires (in the worst case) total simulation time that scales linearly with the inverse absolute error:

$$t_d = \mathcal{O}(|\lambda_d^* - \lambda_0|^{-1}) \quad (8)$$

where d is the corresponding target digit of the search stage.

Proof. Assumption $|x_d^* - x_d(\lambda_0)| < b^{-1}$ is equivalent to:

$$|(\lambda_d^* - \lambda_{LB}^d)b^{-d} - (\lambda_0 - \lambda_{LB}^d)b^{-d}| < b^{-1} \quad (9)$$

$$|\lambda_d^* - \lambda_0| < b^{d-1} \quad (10)$$

$$b^{-d} < \frac{|\lambda_d^* - \lambda_0|^{-1}}{b} \quad (11)$$

As the total simulation time, we take the t_d coefficient of the time evolution block $U = e^{-iHt_d}$ in the last QETU layer, added after the ground state preparation layer, which is $t_d = \frac{c_1}{2}$ for the control-free implementation of QETU. For details refer to Appendix A.

$$t_d = \frac{\pi}{2}b^{-d} < \frac{\pi}{2b}|\lambda_d^* - \lambda_0|^{-1} \quad (12)$$

Hence, simulation time t_d , in the worst case, scales linearly with inverse absolute error $|\lambda_d^* - \lambda_0|^{-1}$. \square

Notice how the main assumption about the success of each search stage in the Theorem is independent of the target precision $|\lambda_d^* - \lambda_0|^{-1}$. This enables us to fix the polynomial degree for each search stage, in expense of longer simulation time.

The $x_d(\lambda_0)$ value corresponding to the ground state energy λ_0 is mapped to a value in $[0, 2]$. If we choose our base $b = 10$, correctly identifying the target digit corresponds to the fuzzy bisection search delivering us an x_d^* estimate that lies in $[x_d(\lambda_0) - 0.1, x_d(\lambda_0) + 0.1]$, indicating an error margin interval of length 0.2 in the x -space. A demonstration of the error margin interval mapped in both x and a -spaces are given in Fig. 3.

In our results, it was comfortably achievable to correctly estimate x_d^* , if we can estimate $a_0 := \cos(\frac{\pi}{2}x_d(\lambda_0))$ up to the second digit after the floating point. With this assumption for the estimation of a_0 , we can see how we can get to any arbitrary target precision if we scale c_1 coefficient up by b and update c_2 depending on the outcome of the previous search at each stage in Table I. It is important to note that a_0 values at each search stage, becomes clustered around $x = 1$ where the slope of $\cos(\frac{\pi}{2}x)$ is the sharpest, hence an interval in x -space, gets mapped to a larger interval in a -space.

This also means that the more successful a certain search stage estimates the eigenvalue, the closer $x_d(\lambda_0)$ value gets mapped to 1 in the next stage, creating a positive feedback loop. This effect of where $x_d(\lambda_0)$ values get mapped to, at different stages of the search is visualized in Fig. 4.

If we consider the effect of quantum depolarizing noise, higher depolarizing probability affects how close we can get to the exact a_0 at each search stage before the search has to be terminated due to success probability falling outside the threshold boundaries. Hence, increasing the tolerable error margin interval length in the a -space this way, allows us to achieve meaningful results even though there is a significant depolarizing probability present in the hardware.

$$\lambda_0 \approx -7.727406\dots$$

d	λ_{d+1}^*	c_1	a_0	a^*	λ_d^*	$ \lambda_d^* - \lambda_0 $
0	-8	π	-0.4152	-0.42	-7.72406	$3.3 \cdot 10^{-3}$
-1	-7.72406	10π	0.4173	0.42	-7.72759	$1.9 \cdot 10^{-4}$
-2	-7.72759	$10^2\pi$	-0.3962	-0.4	-7.72738	$2.64 \cdot 10^{-5}$
-3	-7.72738	$10^3\pi$	0.5961	0.6	-7.727409	$3.1 \cdot 10^{-6}$
-4	-7.727409	$10^4\pi$	0.1036	0.1	-7.7274063	$2.3 \cdot 10^{-7}$

TABLE I. Demonstration of how Adaptive Fuzzy Bisection Search can deliver any arbitrary target precision with the assumption of correct estimation of the exact a_0 value up to the second digit after the floating point.

Here a^* is the estimation result of the respective stage and λ_d^* is the eigenvalue estimate corresponding to it. Search was conducted on base 10.

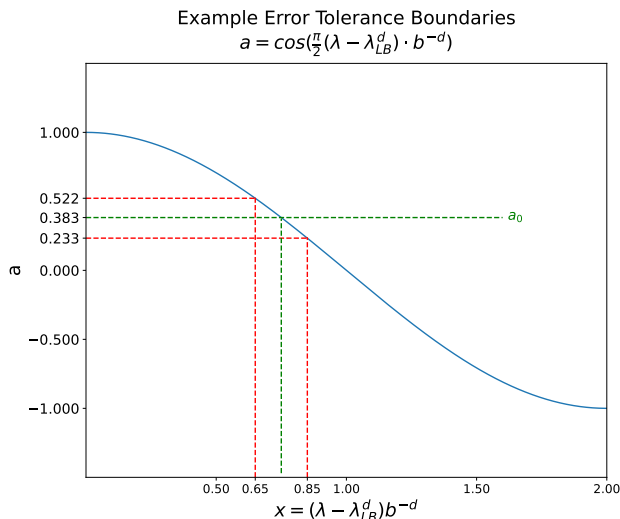


FIG. 3. Mapping of maximum tolerable error margin interval from x -space to a -space in the base $b = 10$; for an example, where $x_d(\lambda_0) = 0.75$. Red lines corresponds to the upper and lower boundaries of the interval and green line represents the exact $x_d(\lambda_0)$ and a_0 values. It is of note that the interval length is larger than 0.2 in a -space, which relaxes the estimation of a_0 compared to our assumption for the demonstration given in Table I.

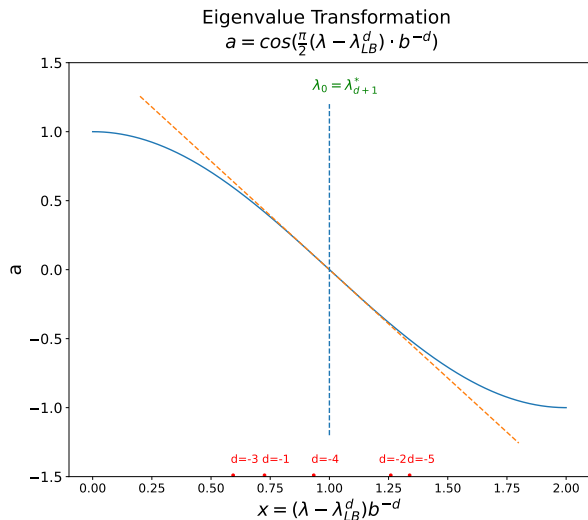


FIG. 4. Example visualization of where $x_d(\lambda_0)$ values are mapped to, for different target digits $d \in \{-5, \dots, -1\}$ in the base $b = 10$. We see that they are clustered around $x = 1$, where the tangent slope of cosine is the sharpest as plotted in orange.

IV. SIMULATION RESULTS

In order to investigate the performance of this approach and compare its results with other ground state energy estimation methods, we ran a set of simulations with IBM `qiskit`. Full implementation can be found

here [11].

We primarily investigated two systems: the transverse-field Ising Model (TFIM) and the Heisenberg model, with respective Hamiltonians

$$H_{\text{TFIM}} = -J \sum_{j=1}^{L-1} Z_j Z_{j+1} - g \sum_{j=1}^L X_j. \quad (13)$$

and

$$H_{\text{Heis}} = - \sum_{j=1}^{L-1} (J_X X_j X_{j+1} + J_Y Y_j Y_{j+1} + J_Z Z_j Z_{j+1}). \quad (14)$$

Moreover, we implemented the QETU circuit with the control-free implementation of the time evolution circuit, as demonstrated in [2, Section VI]. For details of the control-free implementation, see Appendix A.

The ground state is prepared by combining a Lindbladian evolution circuit with a QETU circuit as an amplification layer. Lindbladian evolution circuit is a ground state preparation circuit proposed by Ding et al. [3] to achieve a final overlap of $\langle \psi_0 | \psi_{\text{End}} \rangle > 0$, even though the initial overlap $\langle \psi_0 | \psi \rangle \approx 0$. We use this approach to achieve an initial state for the QETU layer, whose overlap with the ground state is large enough to achieve meaningfully high success probabilities of measuring $|0\rangle$ at the ancilla qubit after applying each QETU layer. This measurement of $|0\rangle$ at the ancilla qubit is necessary to amplify the state fidelity to the ground state, as it can be seen in Formula (1).

After the Lindbladian circuit, we apply QETU to amplify the overlap with the ground state 3 to 5 times and achieve an end state $\langle \psi_{\text{End}} | \psi_0 \rangle \approx 1$.

In order to read out the eigenvalue information from the prepared ground state, we test three different approaches: Direct Expectation Value Measurement (See Appendix B and Appendix E of [2]), Quantum Complex Exponential Least Squares Algorithm (QCELS) [1] and our proposed approach Adaptive Fuzzy Bisection Search. We run our simulations on TFIM Hamiltonian with system sizes of $L = 6$ and $L = 8$ qubits, as well as on Heisenberg Hamiltonian with system sizes $L = 4$ and $L = 6$. Results are investigated for the noiseless case, as well as for (local) depolarizing probability p of 10^{-5} to 10^{-2} . Depolarizing probability p is assumed for two qubit gates and $\frac{p}{10}$ is assumed for single qubit gates.

In order to encode the time evolution operator of system Hamiltonians, we employ primarily three different methods: Second order Trotter-Suzuki decomposition [13], fourth order Blanes-Moan splitting [14] and RQC-Opt. RQC-Opt is an optimization based encoding method, developed by Kotil et al. [12] which uses a Riemannian Trust Region Algorithm to optimize a set of two qubit gates that approximates the time evolution operator of a given Hamiltonian in the brickwall layout. Main idea of this approach is to optimize the gates for smaller systems and use these same gates to encode the time evolution operator of a bigger system with same parameters. This

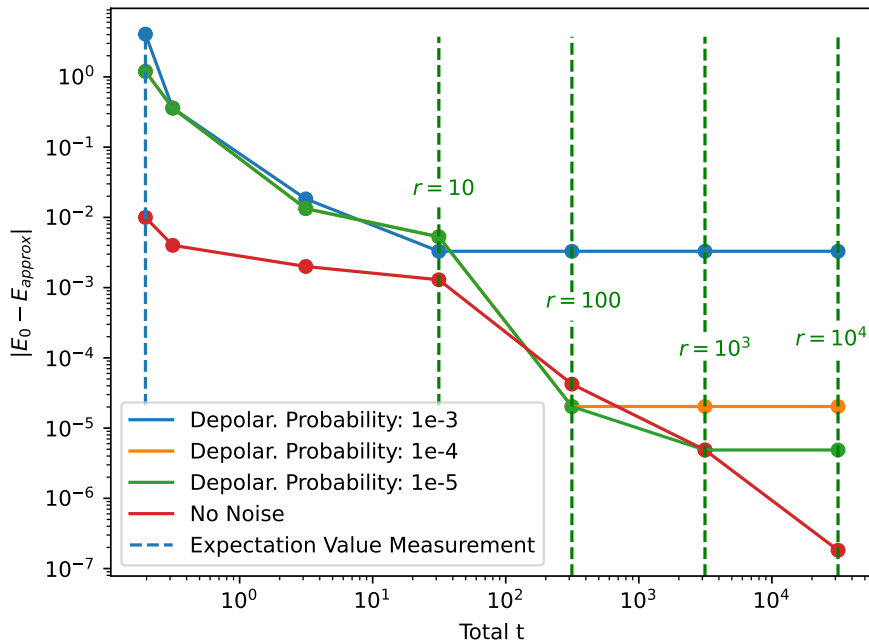


FIG. 5. Ground state energy estimation through Adaptive Fuzzy Bisection Search of TFIM Hamiltonian with system size $L = 8$ and system parameters $J = 1, g = 1$. Time evolution blocks are implemented through RQC-Opt [12], by reusing the optimization results of the smaller system with $L = 6$, hence increasing the circuit depth after a certain target digit. In the graph, r demonstrates the splitting of $dt = \frac{t}{r}$.

method works well for the translation invariant Hamiltonians, allowing us to reach good approximations with shorter circuit depth. It is important to note that us-

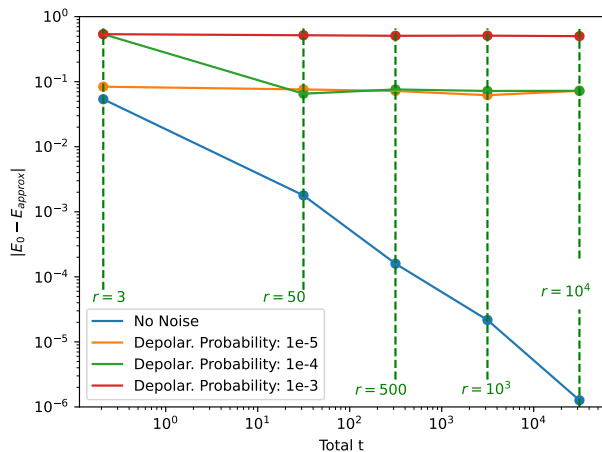


FIG. 6. Ground state energy estimation through Adaptive Fuzzy Bisection Search of Heisenberg Hamiltonian with $L = 4$. Time evolution blocks are implemented through fourth order Blanes-Moan splitting [14]. In the graph r demonstrates the splitting of $dt = \frac{t}{r}$.

ing RQC-Opt algorithm on a smaller system size and reusing the optimized gates for a larger system only works for small enough t coefficients. Empirically this was observed to be equivalent to the condition $t < 10$ for the TFIM with $J = g = 1$ and Heisenberg Hamiltonians with $J_X = J_Y = J_Z = 1$. Simulations visualized in Fig. 5 and Fig. 6 reuse the RQC-Opt results, optimized for a smaller system, hence splits up the total time t in the later search stages. For the details of the simulation of each search stage, please refer to Appendix D.

In Table II, we compare the best results obtained from three different energy estimation methods: Direct Expectation Value Measurement, QCELS Algorithm and Adaptive Fuzzy Bisection Search. Simulation results for the QCELS Algorithm, for different sample sizes N and different depolarizing probabilities are plotted in Fig. 7. In all of the simulations using Adaptive Fuzzy Bisection Search, the search had to terminate exactly one stage earlier when we increased the depolarizing probability by one order of magnitude. From this trend, we formalize the following observation about the relation between the depolarizing probability and absolute error rate.

Observation. *There is a linear trend between the depolarizing probability and minimum achievable absolute error rate:*

$$\min_{d \in \mathbb{Z}} |\lambda_d^* - \lambda_0| = \mathcal{O}(p_{\text{Depolar}}) \quad (15)$$

TFIM, $L = 8$

$p_{Depolar}$	$ \lambda_0 - \lambda^* _{DEM}$	$ \lambda_0 - \lambda^* _{QCELS}$	$ \lambda_0 - \lambda^* _{FBS}$
0	0.0101	$6.286 \cdot 10^{-5}$	$1.286 \cdot 10^{-15}$
10^{-5}	0.024	0.0031	$4.8 \cdot 10^{-6}$
10^{-4}	0.317	0.025	$2.02 \cdot 10^{-5}$
10^{-3}	4.1	0.112	0.0033

Heisenberg, $L = 6$

$p_{Depolar}$	$ \lambda_0 - \lambda^* _{DEM}$	$ \lambda_0 - \lambda^* _{FBS}$
0	0.079	$4.81 \cdot 10^{-11}$
10^{-5}	0.15633	0.15633
10^{-4}	0.3501	0.3501

TABLE II. Ground State Energy Approximation Error lower bounds for TFIM, $L = 8$ and Heisenberg Hamiltonian $L = 6$ under different depolarizing probabilities $p_{Depolar}$. Here $|\lambda_0 - \lambda^*|_{DEM}$ is the result from direct expectation value measurement, $|\lambda_0 - \lambda^*|_{QCELS}$ from the QCELS Algorithm and $|\lambda_0 - \lambda^*|_{FBS}$ from the Adaptive Fuzzy Bisection Search with increasing circuit depth assumption for the time evolution block.

V. DISCUSSION

We see that the Adaptive Fuzzy Bisection approach delivered us a much higher precision for the TFIM Hamiltonian in the sense of having no lower bound for the noiseless case (if ideal ground state preparation is assumed) and reaching its lower bound at a significantly lower absolute error when simulated with depolarizing probability up to 10^{-3} . Lower bound of the results in the noiseless case for Adaptive Fuzzy Bisection Search, as shown in Table II, is resulting from the non-ideal ground state preparation. Major challenge of the Adaptive Fuzzy Bisection approach introduced in this work, is to efficiently implement time evolution blocks with large time steps, as we scale c_1 (hence also T_d) by the search base b after each successful search result, to go into estimating the next digit. Results from simulations of Adaptive Fuzzy Bisection search show that we can reach any arbitrary target precision (assuming perfect ground state preparation) with depolarizing probability up to 10^{-3} , if the circuit depth is kept constant at each search stage. Intuitively, these results provide an upper bound for the error in the noiseless case, even if we do not assume constant circuit depth for the time evolution operator. On the other hand, results of the simulations without assuming constant circuit depth for the time evolution operator are more realistic, as it can be implemented with the existing methods of encoding the time evolution operator and is more likely to be run on Noisy Intermediate-Scale Quantum (NISQ) devices.

Another important thing to note is that this approach does not perform as well, if we run simulations with

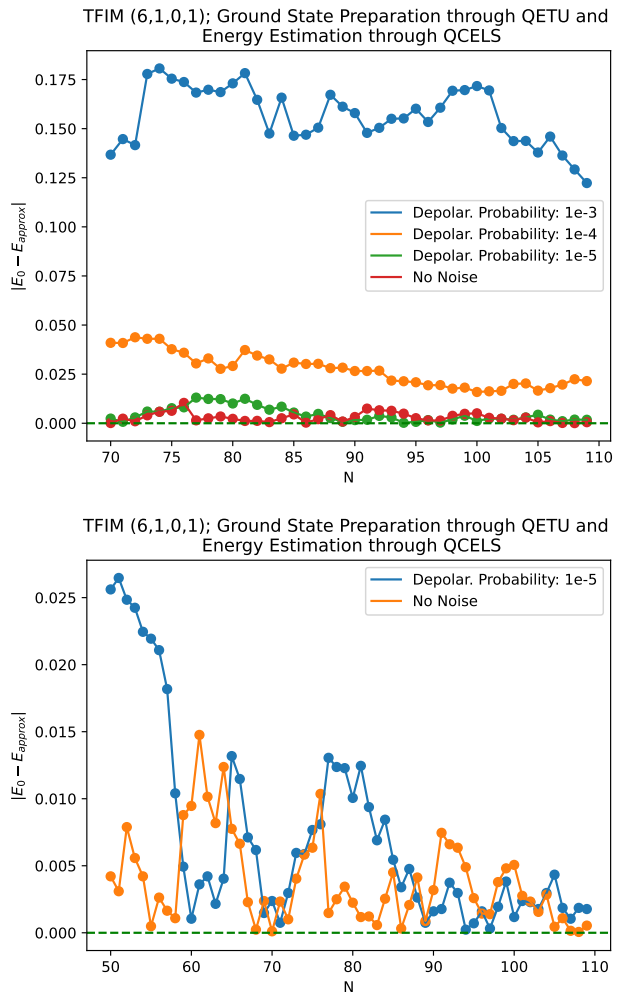


FIG. 7. Ground state energy of TFIM Hamiltonian with system size $L = 6$ and system parameters $J = 1$, $g = 1$, approximated with QCELS [1]. Single time step is set to $\tau = 0.01$. Both real and imaginary parts of the phases are estimated with 10^5 measurements for each Z_n . Optimal θ^* that maximizes $f(\theta)$ was found using `scipy.optimize.fmin`. Top graph demonstrates the approximation process with different depolarizing probabilities $\{10^{-3}, 10^{-4}, 10^{-5}\}$ and without noise. Plots without noise and with depolarizing probability 10^{-5} are magnified in the bottom graph.

Heisenberg model and simulate with noise. The reason for this is the fact that we cannot find a unitary that anti-commutes with the local Heisenberg Hamiltonian which is necessary for the control-free implementation of the QETU Circuit. Hence, we have to start splitting up the total time on much earlier stages as visualized in Fig. 6. This is further explained in Appendix A.1. As splitting t increases circuit depth, the algorithm fails to deliver any significant improvement. In the noiseless case (or depolarizing probability small enough around 10^{-8}), our method still behaves similar to the noiseless simulation of TFIM and does not reach a lower bound if prepared ground state is ideal.

VI. CONCLUSION AND OUTLOOK

We see potential in the future of simulating physics with quantum computers as they can deliver us results which are inefficient to acquire with classical computers for large system sizes. In order to achieve quantum supremacy in this field, there are some primary problems to overcome. One of them is the quantum noise that limits the circuit depth we can introduce and the reliability of the results.

In order to realize the full potential of quantum computing, hardware has to become better to achieve reliable gate fidelity levels, be able to coherently entangle many system qubits at once, as well as reduce systematic and stochastic noise levels to tolerable levels. At the same time, quantum algorithms should be directed towards incorporating error correction methods and enhance noise tolerance.

The novel approach presented in this paper, namely "Adaptive Fuzzy Bisection Search" has been demonstrated to provide an improved error resilience for the systems for which we can find a single Pauli string that anti-commutes with the system Hamiltonian. This approach also performs better when noise levels are taken to be negligibly small. Moreover, this paper can be used as a demonstration of how quantum depolarizing noise affects some of the most popular Hamiltonian simulation algorithms.

In future work, the efficiency and performance of QCELS Algorithm can be investigated for Heisenberg

Hamiltonian with different depolarizing noise levels. Furthermore, circuit optimization methods can be investigated to find a controlled version of the time evolution operator that can be implemented with shorter circuit depth than the methods used in this work, which can enable better noise tolerance and improve the results of simulations with the Heisenberg Hamiltonian.

Methods of efficiently implementing time evolution blocks with large t coefficients should be investigated [15], because the Adaptive Fuzzy Bisection Search introduced in this paper promises a high potential of enhancing noise tolerance, if we can prevent the depth of time evolution circuit from scaling exponentially with increasing time coefficient t .

On top of depolarizing noise, the effects of other noise models, such as amplitude damping [16, 17], dephasing error [18–20], coherent errors in the form of over-rotation [21, 22] and measurement noise [23–25] can be further investigated.

Possibly enhancing our method by combining it with other error correction methods, such as the noise estimation [26], randomized compiling [27] and using a coherent recovery sequence [21, 22] will be our future work.

ACKNOWLEDGMENTS

We would like to thank Lin Lin for insightful discussions during the conceptual development and implementation of this project.

Appendix A: Control-Free Implementation of QETU

The control-free implementation of QETU, requires finding a unitary operator K that anti-commutes with the Hamiltonian:

$$K^\dagger H K = -H \quad (\text{A1})$$

and due to unitarity of K :

$$K^\dagger e^{-iHt} K = e^{iHt}. \quad (\text{A2})$$

So by controlling the unitary K , which can be shown to be a simple Pauli string (hence requiring only single controlled qubit gates) for the Hamiltonians we work with, we can reverse the time evolution in the opposite direction. Due to the symmetry of having $U = e^{-iHt}$ and $U^\dagger = e^{iHt}$ consecutively following each other, we can replace the controlled time evolution by a controlled K gate placed before and after the time evolution operator and scaling the time step by half $\frac{t}{2}$.

For the TFIM Hamiltonian, unitary K can be implemented by using the following simple Pauli string:

$$K_{\text{TFIM}} := Y_1 \otimes Z_2 \otimes Y_3 \dots \quad (\text{A3})$$

For the Heisenberg Hamiltonian, we run into a limitation as there is no single unitary K_{Heis} that can be shown to be anti-commuting with the local Hamiltonian

$$H_{\text{Heis,loc}} := (X \otimes X) + (Y \otimes Y) + (Z \otimes Z) \quad (\text{A4})$$

One way to get around this problem is to split the Hamiltonian into two parts $H_{Heis,1}, H_{Heis,2}$; for which we can find two unitaries $K_{Heis,1}$ and $K_{Heis,2}$ as:

$$H_{Heis,1} := -J_X \sum_{j=1}^{n-1} X_j X_{j+1} - J_Y \sum_{j=1}^{n-1} Y_j Y_{j+1} \quad (A5)$$

$$H_{Heis,2} := -J_Z \sum_{j=1}^{n-1} Z_j Z_{j+1} \quad (A6)$$

with the following unitaries:

$$K_{Heis,1} := Z_1 \otimes I_2 \otimes Z_3 \dots \quad (A7)$$

$$K_{Heis,2} := X_1 \otimes I_2 \otimes X_3 \dots \quad (A8)$$

This has the limitation of having to split the total time t into small enough steps $dt = \frac{t}{r}$, as the following approximation holds only for small enough $\frac{t}{r}$ values:

$$e^{-i\frac{t}{r}(H_1+H_2)} \approx e^{-i\frac{t}{r}H_1} e^{-i\frac{t}{r}H_2} \quad (A9)$$

This implies that we have to increase the circuit depth compared to the implementation of QETU with TFIM Hamiltonian. This effect is visualized in Fig. 8. This additional increase in circuit depth greatly reduces the performance of the adaptive fuzzy bisection search if we use the Heisenberg Hamiltonian as our system compared to its performance with system Hamiltonian as TFIM.

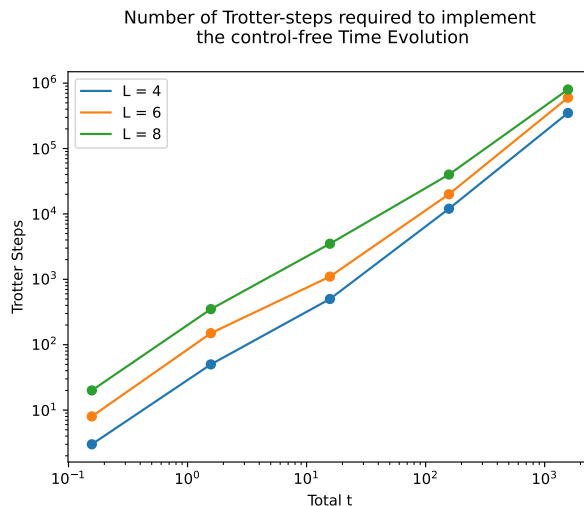


FIG. 8. Number of trotter steps r needed to divide up the total time t , such that the absolute error of the split implementation of Heisenberg Hamiltonian time evolution operator stays below the empirical threshold 0.1. There is a direct correlation between the number of Trotter steps and the circuit depth, hence also with the susceptibility to noise. The graph is plotted for different system sizes (number of qubits) $L \in \{4, 6, 8\}$.

Appendix B: Direct Expectation Value Measurement

The most straightforward and trivial idea of extracting the ground state energy information from the prepared ground state would be to directly conduct measurements on the ground state to approximate the probability distribution of the state vector. This works in cases where the expectation value of the energy can be decomposed into a combination of Pauli operations, which corresponds to calculating the expectation value of the ground

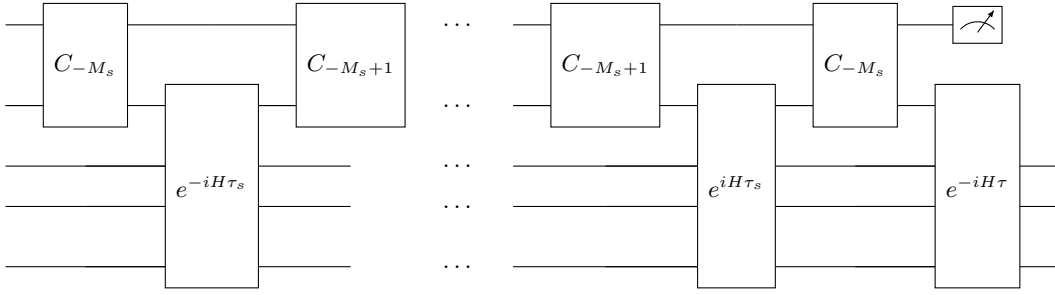


FIG. 9. Lindbladian evolution circuit evolving the input state by one time step τ , implemented by using two qubit gates and small step time evolution τ_s to encode the discretized jump operator, followed by a large step time evolution block. The example circuit corresponds to a system size of four qubits.

state w.r.t. a different measurement basis. This approach inevitably faces a stochastic limit as approximating the probability distribution with high precision for large systems is not possible with a sensible amount of experiments. Hence, the lower bound of approximation error significantly increases with growing system size, even in the ideal, noiseless case.

For the TFIM Hamiltonian, this corresponds to:

$$\begin{aligned}
 E_0 &= \langle \psi_0 | H_{\text{TFIM}} | \psi_0 \rangle = -J \sum_{j=1}^{L-1} \langle \psi_0 | Z_j Z_{j+1} | \psi_0 \rangle - g \sum_{j=1}^L \langle \psi_0 | X_j | \psi_0 \rangle \\
 &= -J \sum_{j=1}^{L-1} \sum_{\sigma_j=0}^1 \sum_{\sigma_{j+1}=0}^1 (-1)^{\sigma_j} (-1)^{\sigma_{j+1}} \mathbb{P}_Z(\sigma_j, \sigma_{j+1} | \psi_0) - g \sum_{j=1}^L \sum_{\sigma_j=0}^1 (-1)^{\sigma_j} \mathbb{P}_X(\sigma_j | \psi_0)
 \end{aligned} \tag{B1}$$

where $\mathbb{P}_X(\sigma_j | \psi_0)$ is the probability of measuring j^{th} qubit as $|\sigma_j\rangle$ on the X -basis and $\mathbb{P}_Z(\sigma_j, \sigma_{j+1} | \psi_0)$ is the probability of measuring j^{th} and $(j+1)^{\text{th}}$ qubits as $|\sigma_j \sigma_{j+1}\rangle$ on the computational basis (Z -basis).

Similarly, the Heisenberg Hamiltonian delivers the following expression:

$$\begin{aligned}
 E_0 &= \langle \psi_0 | H_{\text{Heis}} | \psi_0 \rangle = \sum_{O \in \{X, Y, Z\}} -J_O \sum_{j=1}^{L-1} \langle \psi_0 | O_j O_{j+1} | \psi_0 \rangle \\
 &= \sum_{O \in \{X, Y, Z\}} -J_O \sum_{j=1}^{L-1} \sum_{\sigma_j=0}^1 \sum_{\sigma_{j+1}=0}^1 (-1)^{\sigma_j} (-1)^{\sigma_{j+1}} \mathbb{P}_O(\sigma_j, \sigma_{j+1} | \psi_0)
 \end{aligned} \tag{B2}$$

The simulation of conducting measurements w.r.t. a different basis than the computational basis are made by applying a Hadamard gate to all the qubits for the X -measurement and applying conjugated phase gate and Hadamard gate $S^\dagger H$ to all the qubits for the Y -measurement, due to the following relations:

$$X = HZH, \quad Y = HSZS^\dagger H \tag{B3}$$

Appendix C: Details of Ground State Preparation

This section demonstrates how the ground is prepared for the system Hamiltonians. The main idea is to use the Lindbladian circuit [3] with a relatively small number of time steps to achieve an initial overlap for QETU, which results in reasonable success probabilities of measuring $|0\rangle$ at the ancilla qubit after each QETU layer.

Lindbladian circuit is visualized in Fig. 9. Here, the set of two-qubit gates C_ℓ encode the jump operator K of the Lindbladian evolution as described in Appendix B of [3], and they are implemented as follows:

$$C_\ell := e^{-i \frac{\sqrt{\tau}}{2} \sigma_\ell \otimes A} \tag{C1}$$

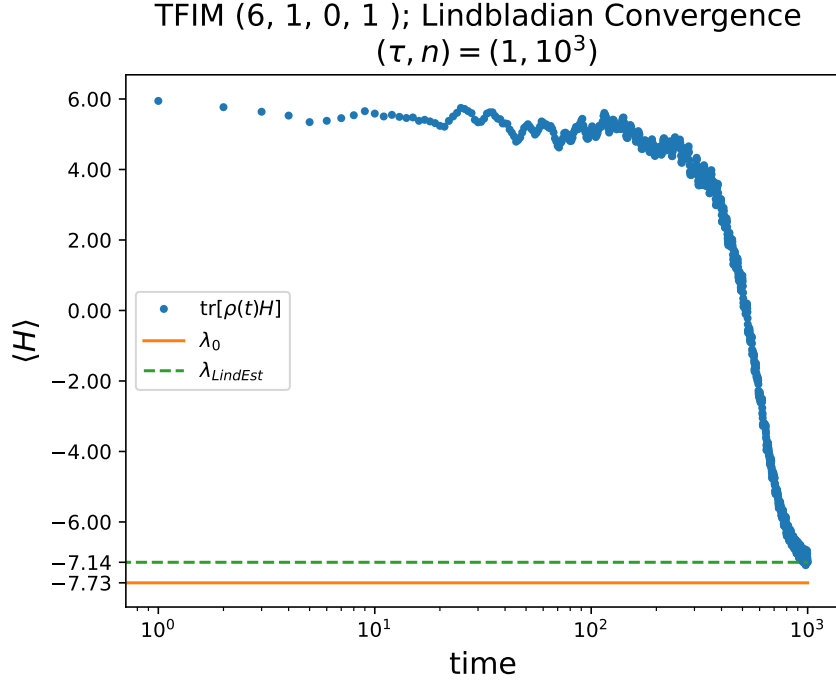


FIG. 10. Convergence of Lindbladian Evolution for TFIM Hamiltonian with system size $L = 6$ and system parameters $J = 1$, $g = 1$. Single time step of the circuit is set to $\tau = 1$ and convergence is simulated for $n = 1000$ steps. Corresponding state fidelity is ≈ 0.729 and absolute error of the eigenvalue corresponding to the prepared state fidelity is ≈ 0.59 .

where τ is the single time step of the Lindbladian evolution, $A \in \mathbb{R}^{2 \times 2}$ is an arbitrary Hermitian matrix and $\sigma_\ell := \tau_s (X \text{Re}\{f(s_\ell)\} + Y \text{Im}\{f(s_\ell)\})$ (X and Y being Pauli matrices). $f(t)$ is a filter function with the defining property of having a spectrum $\hat{f}(\omega)$, such that:

$$\hat{f}(\omega) = 0, \quad \forall \omega \geq 0 \quad (\text{C2})$$

and s_ℓ follows from the discretization of the integral defining K :

$$K := \int_{-\infty}^{\infty} f(t') e^{iHt'} A e^{-iHt'} dt', \quad (\text{C3})$$

with $\tau_s = \frac{S_s}{M_s}$ being the discretization step, $s_\ell = \tau_s \ell$, $\ell \in \{-M_s, \dots, M_s\}$. S_s and M_s are chosen depending on the filter function.

In our simulations, we choose the filter function to be:

$$\hat{f}(\omega) = \frac{1}{2} \text{erf}\left(\frac{\omega + 2.5S_w}{0.5S_w}\right) - \frac{1}{2} \text{erf}\left(\frac{\omega + \Delta}{\Delta}\right) \quad (\text{C4})$$

where erf is the error function, S_w is the Frobenius norm of the Hamiltonian and Δ is the spectral gap $\lambda_1 - \lambda_0$. We discretize the integral definition of K with $\tau_s = 0.05$ and $S_s = 3$.

Fig. 10 contains the convergence plot of applying Lindbladian circuit for the TFIM Hamiltonian.

After the Lindbladian evolution, we amplify the state fidelity by applying the QETU circuit. Here some guesses have to be made, including a lower bound of the ground state energy λ_{LB} and the total spectrum length D . These guesses are used to apply a linear transformation of the Hamiltonian $\tilde{H} = c_1 H + c_2 I$, as the following:

$$c_1 = \frac{\pi}{D}, \quad c_2 = -c_1 \lambda_{LB} \quad (\text{C5})$$

so that the whole spectrum can be mapped to be between $\tilde{\lambda} \in [0, \pi]$. By using the resulting c_1 coefficient, we optimized the time evolution circuit with a t coefficient $t = \frac{c_1}{2}$ (see A.1) through the RQC-Opt algorithm [12]. Moreover, the cut-off value μ between the ground state and the first excited state in the transformed $a = \cos(\frac{\tilde{\lambda}}{2})$

has to be guessed. However, even though μ does not lie in this interval, QETU amplification still works due to the monotonously increasing nature of the step function in $[0, 1]$, just not as efficiently because we would need to apply QETU more times.

In our simulations, the polynomial approximation of the even step function was optimized using `cvxpy.Minimize` for polynomial degree $d = 30$, with Chebyshev polynomials as basis. Symmetric QSP phases were optimized by using `pyqsp` [28].

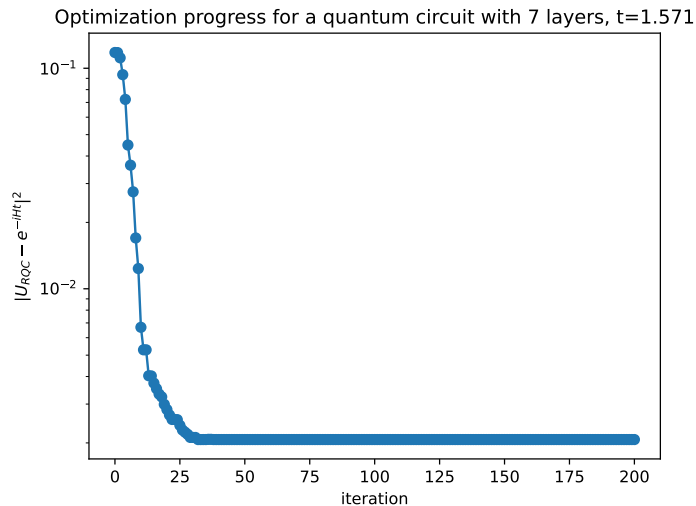


FIG. 11. Optimization of time evolution operator for TFIM Hamiltonian with system size $L = 6$ and system parameters $J = 1, g = 1$; through RQC-Opt, by using 7 layers of two-qubit gates in brickwall layout. Initial error $|U_{RQC} - e^{-iHt}|^2$ is resulting from bootstrapping the optimization by starting the iterations from the previous optimization results, run for 5 layers.

Appendix D: Simulation of Adaptive Fuzzy Bisection Search

In order to start the Adaptive Fuzzy Bisection Search, we need a rough estimate for the eigenvalue, which can be obtained either through the Direct Expectation Value Measurement or the QCELS Algorithm explained in the previous sections. This estimate does not have to meet any certain precision threshold, as the Adaptive Fuzzy Bisection Search can start from any target digit d . We assume in our simulations that we can start with the target digit $d = 0$, corresponding to the first digit after the floating point.

Each single search step of the given search stage is conducted with an additional QETU layer whose symmetric phases $(\phi_0, \phi_1 \dots \phi_1, \phi_0)$ are optimized for the search interval of the search step. We keep the polynomial degree of this QETU layer at 34 for each search step, although this cost can further be reduced by using a lower polynomial degree for the early search steps, due to the larger search interval.

The success probability of measuring $|0\rangle$ at the ancilla qubit is read out by conducting 10^3 measurements for each search step in the early search stages ($d > -2$ for TFIM simulations). This number is increased to 10^4 in the later stages, as the circuit depth starts to scale up due to the Trotter splitting required, as reusing the RQC-Opt [12] to encode the time evolution block works for small enough $dt = \frac{t}{r}$ values, where r is the number of Trotter steps. For the simulations with TFIM $L = 8, J = 1, g = 1$, we observed this condition for t to be: $dt < 10$.

In our simulations with system Hamiltonian selected as TFIM Hamiltonian with system size $L = 8$ and system parameters $J = 1, g = 1$, we assume that we have to reuse the optimization results for the smaller system size. Hence, each Trotter term with $dt < 10$ is implemented with RQC-Opt results, obtained from the optimization with 7 layers of two qubit gates, on TFIM with system size $L = 6$. An example optimization plot for $t = \frac{\pi}{2}$ is given in Fig. 11. We demonstrate the Adaptive Fuzzy Bisection Search stages for target digits $d \in \{-1, -2, -3\}$ in Table IV, for the TFIM Hamiltonian ($L = 8, J = 1, g = 1$) with the aforementioned implementation of the time evolution operator.

As we discussed it in Section IV, our approach can realize its full potential and let us get to any arbitrary target precision with depolarizing probability up to 10^{-3} , if we can efficiently implement the time evolution block with large t coefficients, instead of just using Trotter splittings. The demonstration of how efficiently our method works, if we assume constant circuit depth at each search stage for the time evolution block, is given in Table III for target digits

$d \in \{-2, -3, -4, -5\}$. This simulation is run for the TFIM with system size $L = 6$, by optimizing the time evolution block for the given t at each search stage.

TFIM L=6, $\lambda_0 = -7.727406\dots$
 $d = -2$, $\lambda_{LB}^d = -7.73$, $a_0 \approx 0.417$

μ	l	r	$ F(a_0) ^2$	$\mathbb{P}(0\rangle)$
0.5	0	1	0.0003	0.2423
0.255	0	0.51	0.773	0.6956
0.3775	0.245	0.51	0.6179	0.6082
0.4387	0.3675	0.51	0.089	0.3239
0.4081	0.3675	0.44875	0.263	0.4193

$$\lambda_d^* \approx -7.72706, \quad |\lambda_d^* - \lambda_0| \approx 3 \cdot 10^{-4},$$

$$d = -3, \lambda_{LB}^d = -7.72806, a_0 \approx 0.596$$

μ	l	r	$ F(a_0) ^2$	$\mathbb{P}(0\rangle)$
0.5	0	1	0.889	0.7444
0.745	0.49	1	0.003	0.2391
0.6225	0.49	0.755	0.059	0.2877
0.56125	0.49	0.6325	0.562	0.5682

$$\lambda_d^* \approx -7.727379, \quad |\lambda_d^* - \lambda_0| \approx 2 \cdot 10^{-5},$$

$$d = -4, \lambda_{LB}^d = -7.727479, a_0 \approx 0.104$$

μ	l	r	$ F(a_0) ^2$	$\mathbb{P}(0\rangle)$
0.5	0	1	0.0002	0.2444
0.255	0	0.51	0.0026	0.2689
0.1325	0	0.265	0.0556	0.3048
0.071	0	0.1425	0.5051	0.5402

$$\lambda_d^* \approx -7.72740451, \quad |\lambda_d^* - \lambda_0| \approx 2 \cdot 10^{-6},$$

$$d = -5, \lambda_{LB}^d = -7.72741, a_0 \approx 0.861$$

μ	l	r	$ F(a_0) ^2$	$\mathbb{P}(0\rangle)$
0.5	0	1	0.87091	0.7155
0.745	0.49	1	0.7931	0.6599
0.8675	0.735	1	0.155	0.2877
0.8062	0.735	0.8775	0.888	0.6957
0.83687	0.79624	0.8775	0.6410	0.5586

$$\lambda_d^* \approx -7.7274063, \quad |\lambda_d^* - \lambda_0| \approx 3 \cdot 10^{-7},$$

TABLE III. Adaptive Fuzzy Bisection Search stages, demonstrated for target digits $d \in \{-2, -3, -4, -5\}$, under depolarizing probability of 10^{-3} . Note that constant circuit depth for time evolution block is assumed at each stage, as time evolution circuit was optimized for the system size $L = 6$. Threshold success probability boundaries to end the search are set as $[0.4, 0.6]$. Each experiment is conducted with 10^5 measurements on ancilla qubit.

TFIM L=8, $\lambda_0 = -10.251661\dots$
 $d = 0$, $r=1$, $\lambda_{LB}^d = -11$, $a_0 \approx 0.3253$

μ	l	r	$ F(a_0) ^2$	$\mathbb{P}(0\rangle)$
0.5	0	1	0.01	0.1
0.25	0	0.51	0.83	0.78
0.375	0.249	0.51	0.61	0.52

$$\lambda_d^* \approx -10.281413, \quad |\lambda_d^* - \lambda_0| \approx 3 \cdot 10^{-2},$$

$$d = -1, r=10, \lambda_{LB}^d = -10.381413, a_0 \approx 0.7253$$

μ	l	r	$ F(a_0) ^2$	$\mathbb{P}(0\rangle)$
0.5	0	1	0.889	0.62
0.745	0.49	1	0.23	0.367
0.6225	0.49	0.755	0.632	0.542

$$\lambda_d^* \approx -10.248368, \quad |\lambda_d^* - \lambda_0| \approx 3 \cdot 10^{-3},$$

$$d = -2, r=100, \lambda_{LB}^d = 10.258368, a_0 \approx 0.258$$

μ	l	r	$ F(a_0) ^2$	$\mathbb{P}(0\rangle)$
0.5	0	1	0.00020	0.51561

TABLE IV. Adaptive Fuzzy Bisection Search stages, demonstrated for target digits $d \in \{0, -1, -2\}$, under depolarizing probability of 10^{-3} . Note that circuit depth scales by 10 at each search stage as time evolution operator is not optimized for the system size $L = 8$ but optimization results from $L = 6$ were reused. Threshold success probability boundaries to end the search are set as $[0.4, 0.6]$. Each experiment is conducted with 10^3 measurements on ancilla qubit.

REFERENCES

- [1] Z. Ding and L. Lin, Even shorter quantum circuit for phase estimation on early fault-tolerant quantum computers with applications to ground-state energy estimation, *PRX Quantum* **4**, 020331 (2023).
- [2] Y. Dong, L. Lin, and Y. Tong, Ground-state preparation and energy estimation on early fault-tolerant quantum computers via quantum eigenvalue transformation of unitary matrices, *PRX Quantum* **3**, 040305 (2022).
- [3] Z. Ding, C.-F. Chen, and L. Lin, Single-ancilla ground state preparation via Lindbladians, arXiv:2308.15676 (2023), arXiv:2308.15676 [quant-ph].
- [4] D. Layden, First-order Trotter error from a second-order perspective, *Phys. Rev. Lett.* **128**, 210501 (2022).
- [5] L. Lin and Y. Tong, Heisenberg-limited ground-state energy estimation for early fault-tolerant quantum computers, *PRX Quantum* **3**, 010318 (2022).
- [6] K. Wan, M. Berta, and E. T. Campbell, Randomized quantum algorithm for statistical phase estimation, *Phys. Rev. Lett.* **129**, 030503 (2022).
- [7] G. Wang, S. Sim, and P. D. Johnson, State preparation boosters for early fault-tolerant quantum computation, *Quantum* **6**, 829 (2022).
- [8] R. Zhang, G. Wang, and P. Johnson, Computing ground state properties with early fault-tolerant quantum computers, *Quantum* **6**, 761 (2022).
- [9] G. H. Low and I. L. Chuang, Optimal Hamiltonian simulation by quantum signal processing, *Phys. Rev. Lett.* **118**, 010501 (2017).
- [10] J. M. Martyn, Z. M. Rossi, A. K. Tan, and I. L. Chuang, Grand unification of quantum algorithms, *PRX Quantum* **2**, 040203 (2021).
- [11] E. Karacan, Noise tolerant ground state energy estimation through quantum eigenvalue transformation of unitary matrices (QETU).
- [12] A. Kotil, R. Banerjee, Q. Huang, and C. B. Mendl, Riemannian quantum circuit optimization for Hamiltonian simulation, *J. Phys. A: Math. Theor.* **57**, 135303 (2024).
- [13] M. Suzuki, General theory of fractal path integrals with applications to many-body theories and statistical physics, *J. Math. Phys.* **32**, 400 (1991).
- [14] S. Blanes and P. C. Moan, Practical symplectic partitioned Runge-Kutta and Runge-Kutta-Nyström methods, *J. Comput. Appl. Math.* **142**, 313 (2002).
- [15] C. Mc Keever and M. Lubasch, Classically optimized Hamiltonian simulation, *Phys. Rev. Res.* **5**, 023146 (2023).
- [16] M. A. Nielsen and I. L. Chuang, *Quantum Computation and Quantum Information* (Cambridge University Press, 2010).
- [17] M. A. Aziz, B. P. Gond, S. Nandi, S. Ray, D. Bhounik, and R. Majumdar, Thermal relaxation error on QKD: effect and a probable bypass, arXiv:2207.01159 (2022), arXiv:2207.01159 [quant-ph].
- [18] I. L. Chuang, R. Laflamme, P. W. Shor, and W. H. Zurek, Quantum computers, factoring, and decoherence, *Science* **270**, 1633 (1995).
- [19] A. Barenco, A. Ekert, K.-A. Suominen, and P. Törmä, Approximate quantum Fourier transform and decoherence, *Phys. Rev. A* **54**, 139 (1996).
- [20] W. G. Unruh, Maintaining coherence in quantum computers, *Phys. Rev. A* **51**, 992 (1995).
- [21] A. K. Tan, Y. Liu, M. C. Tran, and I. L. Chuang, Error correction of quantum algorithms: arbitrarily accurate recovery of noisy quantum signal processing, arXiv:2301.08542 (2023), arXiv:2301.08542 [quant-ph].
- [22] A. K. Tan, Y. Liu, M. C. Tran, and I. L. Chuang, Perturbative model of noisy quantum signal processing, *Phys. Rev. A* **107**, 042429 (2023).
- [23] F. Wudarski, Y. Zhang, and M. I. Dykman, Nonergodic measurements of qubit frequency noise, *Phys. Rev. Lett.* **131**, 230201 (2023).
- [24] F. Wudarski, Y. Zhang, A. N. Korotkov, A. G. Petukhov, and M. I. Dykman, Characterizing low-frequency qubit noise, *Phys. Rev. Applied* **19**, 064066 (2023).
- [25] B. Nachman, M. Urbanek, W. A. de Jong, and C. W. Bauer, Unfolding quantum computer readout noise, *npj Quantum Inf.* **6**, 84 (2020).
- [26] M. Urbanek, B. Nachman, V. R. Pascuzzi, A. He, C. W. Bauer, and W. A. de Jong, Mitigating depolarizing noise on quantum computers with noise-estimation circuits, *Phys. Rev. Lett.* **127**, 270502 (2021).
- [27] A. Hashim, R. K. Naik, A. Morvan, J.-L. Ville, B. Mitchell, J. M. Kreikebaum, M. Davis, E. Smith, C. Iancu, K. P. O'Brien, I. Hincks, J. J. Wallman, J. Emerson, and I. Siddiqi, Randomized compiling for scalable quantum computing on a noisy superconducting quantum processor, *Phys. Rev. X* **11**, 041039 (2021).
- [28] R. Chao, D. Ding, A. Gilyen, C. Huang, and M. Szegedy, Finding angles for quantum signal processing with machine precision, arXiv:2003.02831 (2020), arXiv:2003.02831 [quant-ph].